crystals

Article

Luminescence Investigation of $BaMgF_4$ Ceramics Under VUV Synchrotron Excitation

Amangeldy M. Zhunusbekov [1], Assel V. Strelkova [1], Zhakyp T. Karipbayev [1,*], Kuat K. Kumarbekov [1], Abdirash Akilbekov [1], Raigul N. Kassymkhanova [1,*], Murat T. Kassymzhanov [1], Yevheniia Smortsova [2] and Anatoli I. Popov [1,3]

[1] Institute of Physical and Technical Sciences, L.N. Gumilyov Eurasian National University, Astana 010008, Kazakhstan; zhunusbekov_am@enu.kz (A.M.Z.); a.strelkova@nurorda.kz (A.V.S.); kumarbekov_kk_1@enu.kz (K.K.K.); kassymzhanov_mt@enu.kz (M.T.K.); popov@latnet.lv (A.I.P.)
[2] Deutsches Elektronen-Synchrotron DESY, 22603 Hamburg, Germany; akilbekov_at@enu.kz (A.A.); yevheniia.smortsova@desy.de (Y.S.)
[3] Institute of Solid State Physics, University of Latvia, 8 Kengaraga, LV-1063 Riga, Latvia
* Correspondence: karipbayev_zht_1@enu.kz (Z.T.K.); suleimen_rn@enu.kz (R.N.K.)

Abstract: The luminescence properties of $BaMgF_4$ ceramics synthesized using electron beam-assisted synthesis were investigated under vacuum ultraviolet (VUV) synchrotron excitation at a cryogenic temperature of T = 9 K. Their excitation spectra, measured over the 4–10.8 eV range, and corresponding luminescence spectra revealed a complex multi-component structure with emission maxima at 3.71, 3.55, 3.33, 3, and ~2.8 eV. The primary luminescence band at 330 nm was attributed to self-trapped excitons (STE) excited near the band edge (9.3–9.7 eV), indicating interband transitions and subsequent excitonic relaxation. Bands at 3 and ~2.8 eV were associated with defect states efficiently excited at 6.45 eV, 8 eV and high-energy transitions near 10.3 eV. The excitation spectrum showed distinct maxima at 5, 6.45, and 8 eV, which were interpreted as excitations of defect-related states. These results highlight the interplay between interband transitions, excitonic processes, and defect-related luminescence, which defines the complex dynamics of $BaMgF_4$ ceramics. These findings confirm that radiation synthesis introduces defect centers influencing luminescent properties, making $BaMgF_4$ a promising material for VUV and UV applications.

Keywords: barium magnesium fluoride; ceramics; VUV excitation

check for updates

Academic Editor: Feng Gao

Received: 21 December 2024
Revised: 20 January 2025
Accepted: 21 January 2025
Published: 24 January 2025

Citation: Zhunusbekov, A.M.; Strelkova, A.V.; Karipbayev, Z.T.; Kumarbekov, K.K.; Akilbekov, A.; Kassymkhanova, R.N.; Kassymzhanov, M.T.; Smortsova, Y.; Popov, A.I. Luminescence Investigation of $BaMgF_4$ Ceramics Under VUV Synchrotron Excitation. *Crystals* **2025**, *15*, 127. https://doi.org/10.3390/cryst15020127

1. Introduction

$BaMgF_4$ (barium magnesium fluoride) crystals represent a promising material with a wide range of applications. $BaMgF_4$ exhibits excellent transparency and high radiation resistance across the ultraviolet/vacuum ultraviolet (UV/VUV) to infrared (IR) range. Furthermore, these crystals can undergo periodic poling (PP) to facilitate second harmonic generation (SHG) using quasi-phase-matching (QPM) techniques [1]. Due to their nonlinear optical effects, $BaMgF_4$ crystals are emerging as promising candidates for tunable laser materials [2].

$BaMgF_4$ has garnered significant interest in the field of multiferroics—materials that exhibit both ferroelectric and ferromagnetic properties [3,4]. Nd^{3+}-doped $BaMgF_4$ is a ferroelectric material with exceptional transparency, making it a potential candidate for optical devices operating in the UV/VUV and mid-IR spectral ranges [5]. While there has been some research on the optical properties of $BaMgF_4$ doped with divalent and trivalent europium ions, these studies have predominantly focused on thin films or glass substrates, with limited investigations into luminescent or upconversion properties [6,7]. The work in [8] extends the study of upconversion properties in $BaMgF_4$:Yb^{3+} and Er^{3+} phosphors, demonstrating a flexible approach to tuning the emission color from green to red.

Among various ferroelectric fluoride crystals, $BaMgF_4$ stands out due to its transparency in the deep ultraviolet range. Studies [9] have explored its properties for use in UV and VUV nonlinear optical applications. However, its transparency decreases as the wavelength approaches the cutoff around 130 nm, which is attributed to the presence of scattering centers.

$BaMgF_4$ crystals are known for their wide bandgap and ultrafast valence emission in the 190–220 nm range [10]. There is growing interest in Ce^{3+}-doped crystals, especially for use in visible-range scintillators and tunable UV lasers [11]. Single crystals of $BaMgF_4$ exhibit intense luminescence with a peak near 205 nm when exposed to X-rays, with an absolute light yield of 1300 photons/MeV and a bi-exponential decay with lifetimes of 0.57 ± 0.01 ns (70%) and 2.27 ± 0.31 ns (30%) at room temperature [12].

The authors of [13] investigated the spectral-luminescent properties of Nd^{3+}-doped $BaMgF_4$ using synchrotron radiation in the VUV range. $BaMgF_4$ serves as an excellent matrix for rapid and efficient 5d–4f luminescence of Nd^{3+} ions without suffering from thermal quenching of luminescence over the 8–300 K temperature range.

In [14], the luminescence of $SrMgF_4$ single crystals was studied under synchrotron radiation excitation in the VUV region. $SrMgF_4$, which shares a typical fluoride crystal structure, demonstrated that lattice defects play a key role in these luminescence processes. Luminescence bands in the 1.8–2.6 eV and 4.2–5.5 eV regions were linked to the relaxation of excited states associated with these defects.

The potential of metal fluoride crystals in advanced optical applications was further emphasized by an important study, which successfully grew $BaMgF_4$ crystals and conducted detailed investigations of their crystal optical properties [15–27]. The wide variety of applications for luminescent materials based on metal fluorides has necessitated the development of various synthesis technologies. The synthesis of $BaMgF_4$ with activators is a complex process requiring precise control of various parameters and temperature. The challenges in synthesizing metal fluorides are primarily due to the unique properties of fluorine. As such, the synthesis of metal fluorides involves a complex technological chain of operations performed at high temperatures.

In our work, we synthesized $BaMgF_4$ ceramics using a radiation-assisted method, employing a powerful electron beam [28–30]. Radiation synthesis occurs without the use of additives or additional treatments. Compared to other methods, this technique does not require additional precursors. We studied the electronic excitations and luminescence of the synthesized $BaMgF_4$ ceramics under synchrotron radiation excitation in the VUV region.

The main goal of this work was to investigate the luminescence of intrinsic defects under vacuum ultraviolet (VUV) synchrotron excitation. This study focused on understanding the luminescence mechanisms associated with deep electronic transitions and defect states that are often inaccessible with conventional excitation sources, as they play a critical role in the optical and electronic properties of materials. The results of this investigation will provide valuable insights into the behavior of intrinsic defects in the material and their influence on overall luminescent performance.

2. Materials and Methods

$BaMgF_4$ ceramics were synthesized using a novel technique called electron beam-assisted synthesis (EBAS), an advanced method for producing refractory and intricate compounds. To synthesize $BaMgF_4$ ceramics, high-grade barium fluoride (BaF_2) and magnesium fluoride (MgF_2) with 4N purity, provided by Hebei Suoyi New Material

Technology Co., Ltd. (Handan, China), were utilized as raw materials. These ingredients were accurately weighed in the stoichiometric proportions of 73.84% BaF_2 and 26.16% MgF_2. They were thoroughly mixed in an alumina ball mill to achieve a uniform blend, ensuring even distribution of materials for the ensuing sintering phase.

The synthesis process involved the direct irradiation of the prepared mix using an electron beam with an energy of 1.3 MeV and a power density of 45 W/cm^2 for 180 min, employing the ELV-4 accelerator at the Nuclear Technology Park of L.N. Gumilyov Eurasian National University. Post irradiation, ceramic samples were cooled down to ambient temperature.

Characterization of the synthesized materials was performed using X-ray diffraction (XRD) with a Bruker D6 PHASER, and morphological and elemental analyses were executed using a Tabletop Microscope TM4000Plus II (Hitachi, Tokyo, Japan) equipped with energy-dispersive X-ray spectroscopy (EDS).

Luminescence experiments were conducted at the Superlumi/P66 beamline at DESY's PETRA III synchrotron facility in Hamburg, Germany, as noted in reference [31]. The synchrotron radiation used provided high-intensity, adjustable excitation across the necessary spectral range, with accurate wavelength selection achieved via a 2 m monochromator with a spectral resolution of 4 Å. This setup precisely excited luminescent states in the ceramic samples. The luminescence apparatus at DESY has been extremely effective for researchers focusing on the VUV spectral range [32–35].

Measurements were conducted with a 0.3 m Kymera 328i monochromator (Oxford Instruments Andor Ltd., Bristol, UK) featuring an F/4.1 aperture, covering a spectral range of 200–1200 nm, and offering a spectral resolution of 0.4 nm. A Newton 920 CCD camera (Oxford Instruments Andor Ltd., Bristol, UK) ensured highly sensitive detection across a broad spectral range, while a Hamamatsu R6358 photomultiplier tube (Hamamatsu Photonics, Japan) enabled efficient photon counting, particularly in the ultraviolet range. For luminescence measurements, ceramic samples were carefully cleaved into smaller pieces with smooth surfaces. All measurements were conducted at a cryogenic temperature of 9 K using a helium-cooled cryostat to minimize thermal noise and non-radiative losses. Excitation spectra were calibrated against the sodium salicylate signal, ensuring accurate and reliable data collection across the entire spectral range.

3. Experimental Results and Discussion

3.1. SEM, EDS, and XRD Analysis

After synthesis, investigations of morphology, energy-dispersive spectroscopy (EDS) (Figure 1), and X-ray diffraction (XRD) (Figure 2) were conducted. In Figure 1a, obtained using scanning electron microscopy (SEM) at a magnification of 3000× (Figure 1a), the microstructure of $BaMgF_4$ ceramics is revealed. The image displays a porous structure, where dark regions likely correspond to porous or lower-density areas of the material, while brighter regions represent denser areas. The formation of such a structure may be attributed to the impact of high-energy electrons, which cause localized changes in material density, leading to the generation of pores and microcracks. These microstructural features could also result from the rapid synthesis process, where the formation of dense grains coexists with areas of lower density.

Pore sizes in $BaMgF_4$ ceramics observed in the SEM image ranged from approximately 0.5 to 1 μm. These pores may serve as evidence of fluorine ionization processes or the volatilization of lightweight fluorine compounds under electron beam irradiation. High-energy electrons are capable of displacing light fluorine atoms from the lattice, thereby leading to the formation of defects and voids in the material.

EDS analysis results are presented in Figure 1b,c. The spectrum confirms the presence of all constituent elements of $BaMgF_4$, specifically Ba, Mg, and F. However, the intensities of these peaks indicate variations in elemental content, which may suggest inhomogeneous distribution within the sample or deviations from ideal stoichiometry. These EDS results highlight a deficiency of fluorine and its uneven distribution in the ceramic structure.

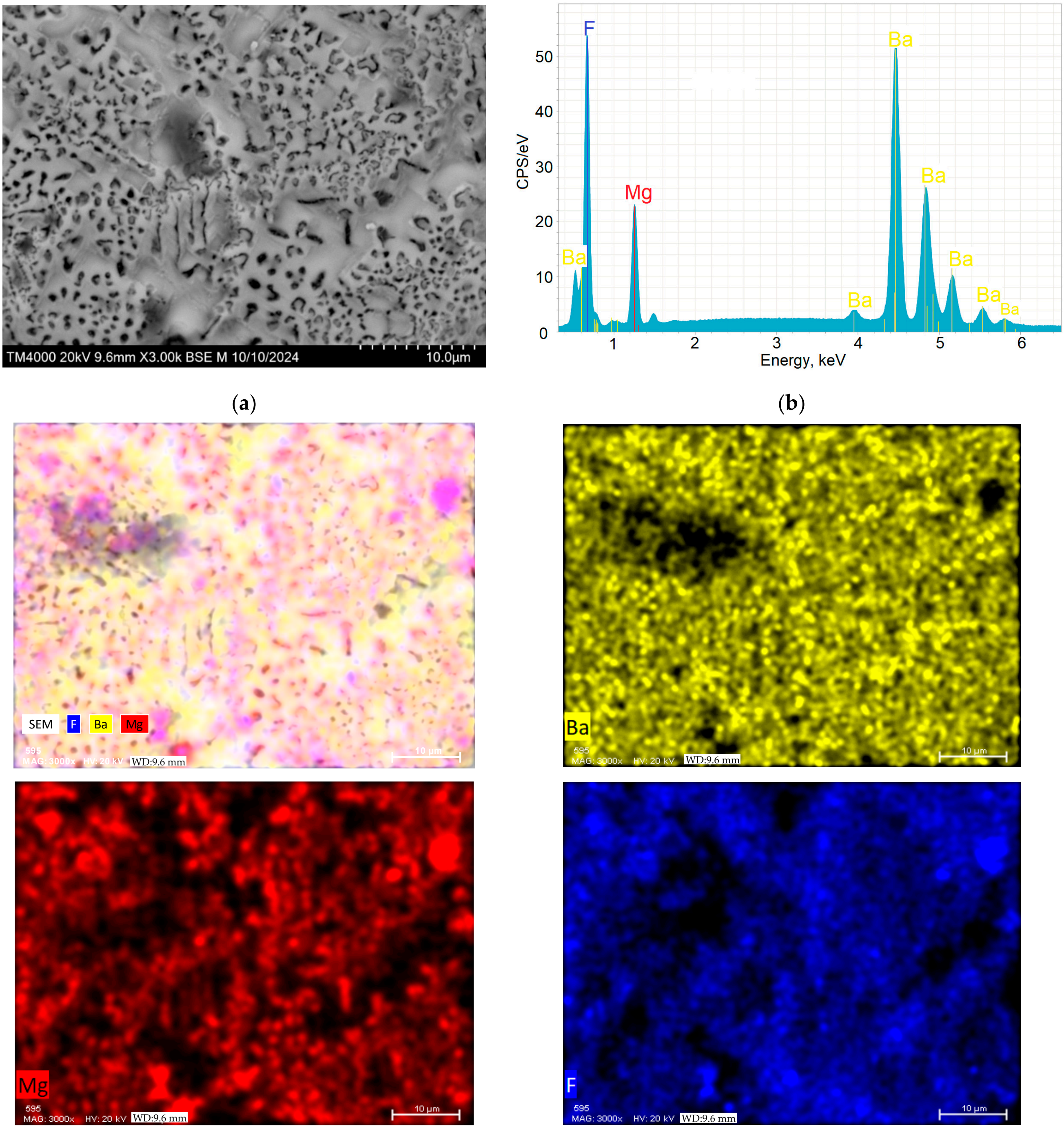

(**a**)

(**b**)

(**c**)

Figure 1. SEM image (**a**), EDS spectra (**b**), and elemental mapping (**c**) of $BaMgF_4$ ceramics.

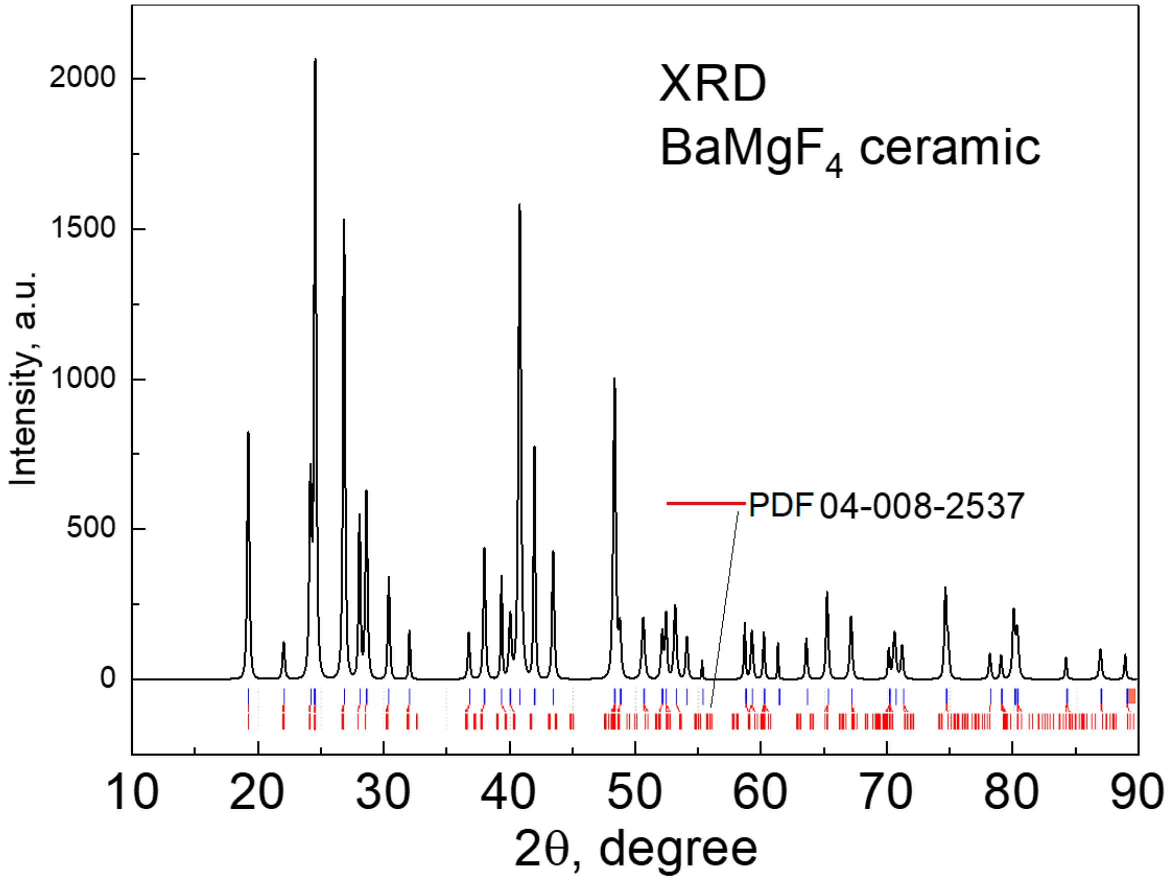

Figure 2. XRD pattern of $BaMgF_4$ ceramic (black line—measured diffractogram, blue lines—XRD peak positions, red lines—reference form PDF database).

The observed fluorine deficiency on the ceramic surface can be attributed to multiple factors: the synthesis, which is completed within approximately one minute, limits the diffusion and stabilization of fluorine in the lattice; during high-energy electron beam synthesis, volatile fluorine compounds may form due to the interaction of the electron beam with the material, resulting in partial fluorine loss; and conducting synthesis in an air environment facilitates potential reactions between fluorine and atmospheric oxygen, leading to fluorine volatilization or oxidation processes.

Structural studies of $BaMgF_4$ ceramics were conducted using X-ray diffraction (XRD), as shown in Figure 2. The XRD analysis confirmed the presence of the primary $BaMgF_4$ phase as the dominant component. Phase identification was carried out using the PDF-4+ 2019 database, with phase matching performed against reference cards. Specifically, the database reference card 04-008-2537 was used for the identification of the $BaMgF_4$ phase.

Profile parameters were calculated using the B-spline model for background correction, with considerations for peak asymmetry and broadening factors to ensure accurate data refinement. The XRD analysis revealed the following structural and crystallographic parameters for $BaMgF_4$ ceramics: the compound crystallizes in the orthorhombic $Cmc2_1$ space group with lattice constants a = 4.14 Å, b = 14.56 Å, and c = 5.83 Å, along with an interaxial angle of $\alpha = 90^\circ$. The calculated unit cell volume is 351 $Å^3$, and the material's density is 4.490 g/cm^3, indicating excellent structural consistency.

The crystallite size was 41.4 nm. Phase composition analysis revealed that the $BaMgF_4$ phase constituted 99.31% of the material, confirming its exceptional phase purity and uniformity.

The $BaMgF_4$ phase exhibited an orthorhombic structure, with lattice parameters that closely approximated a cubic arrangement due to the proportional relationships between lattice constants and inherent symmetry.

The orientation parameters and crystalline structure, as well as the calculated space group, demonstrated excellent agreement with theoretical models and previously reported data for these phases. These results confirmed the successful synthesis of high-purity $BaMgF_4$ ceramics with well-defined structural and physical characteristics.

One of the key novelties of this study was the ability to synthesize $BaMgF_4$ on the ELV-4 installation using high-energy electron irradiation at an energy of 1.3 MeV, combined with a significantly reduced power density of 45 W/cm^2 and an extended exposure time of 180 min. This approach stands in stark contrast to previously reported conditions [28–30,36–38], which were carried out on the ELV-6 installation with an energy of 1.4 MeV, a much higher power density of 20–25 kW/cm^2, and an extremely short exposure time of approximately 1 s. This methodology not only opens new possibilities for controlling the synthesis parameters of fluoride materials but also establishes the lower limits of conditions under which successful ceramic formation can occur by this technology.

3.2. Luminescence Study Under VUV Excitation

To investigate the luminescent properties of the synthesized $BaMgF_4$ ceramics, studies were conducted in the ultraviolet (UV) to vacuum ultraviolet (VUV) regions, covering an excitation energy range from 4 to 10.8 eV. Results are presented as a 3D mapping of luminescent characteristics at a temperature of $T = 9$ K (Figure 3). This study of the luminescent properties of $BaMgF_4$ ceramics at 9 K was primarily driven by the necessity to minimize phonon scattering and non-radiative losses, which can obscure the intrinsic luminescent properties of the material. At cryogenic temperatures, relaxation mechanisms such as phonon interactions are significantly suppressed, allowing for the precise detection of luminescence arising from self-trapped excitons (STE) and defect-related states.

In the 3D map (Figure 3) of the central graph, the vertical axis represents the excitation energy (in eV), while the horizontal axis corresponds to the emission wavelength (in nanometers). Each colored pixel on the graph indicates the luminescence intensity at a specific combination of excitation energy and emission wavelength.

At low temperatures, $BaMgF_4$ ceramics exhibited strong luminescence over a broad spectral range from 300 to 550 nm. These photoluminescence (PL) spectra revealed distinct maxima at emission wavelengths of 336, 372, 420, and 470 nm. The overall trends of the luminescence intensity as a function of excitation energy were as follows: as the excitation energy increased from 4 to 10.8 eV, the PL intensity gradually changed across the spectrum. In all cases, the primary maximum was observed at 336 nm. Notably, with increasing excitation energy, the intensity at 336 nm increased, while the intensity at 420 nm decreased simultaneously.

At higher excitation energies (9.7–10.3 eV), intense peaks were observed for the emission wavelength 336 nm (Figure 4). Peaks at 9.7 and 10.3 eV were also present for the emission wavelength 372 nm, but their intensity was notably lower compared to 336 nm, indicating less efficient excitation of the centers responsible for this emission.

In the mid-energy range (6.45–8 eV) (Figure 4), the excitation spectrum showed pronounced peaks for emission wavelengths 336 nm and 372 nm, suggesting the excitation of intermediate states or excitonic levels associated with the interaction between the electron-hole pair and the crystal lattice. For longer emission wavelengths, such as 420 nm and 470 nm, the intensity in this region was significantly lower, indicating a weaker contribution of these transitions to emission at longer wavelengths.

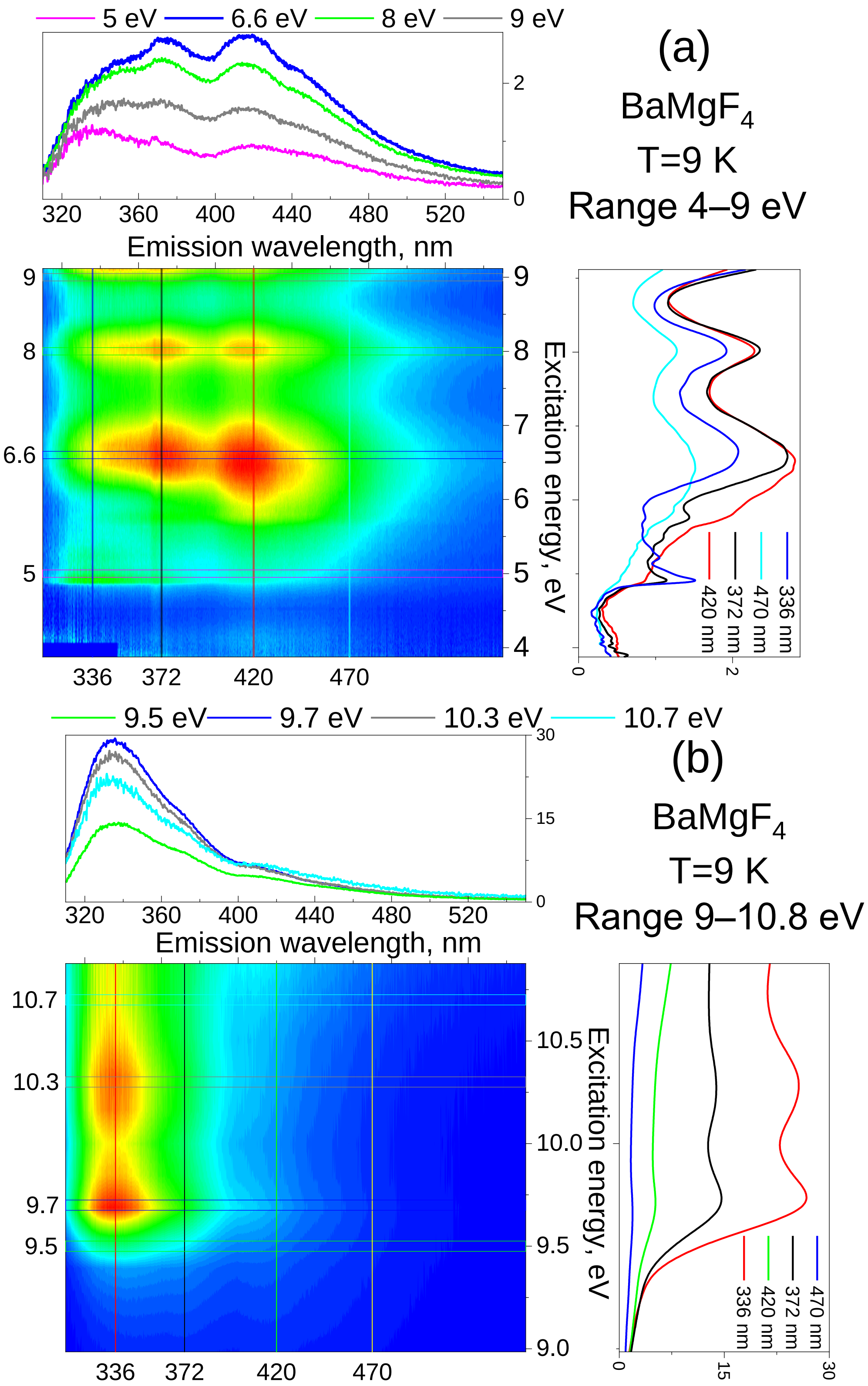

Figure 3. $BaMgF_4$ ceramics 3D luminescence/excitation mapping: (**a**) for the range 4–9 eV, (**b**) for the range 9–10.8 eV.

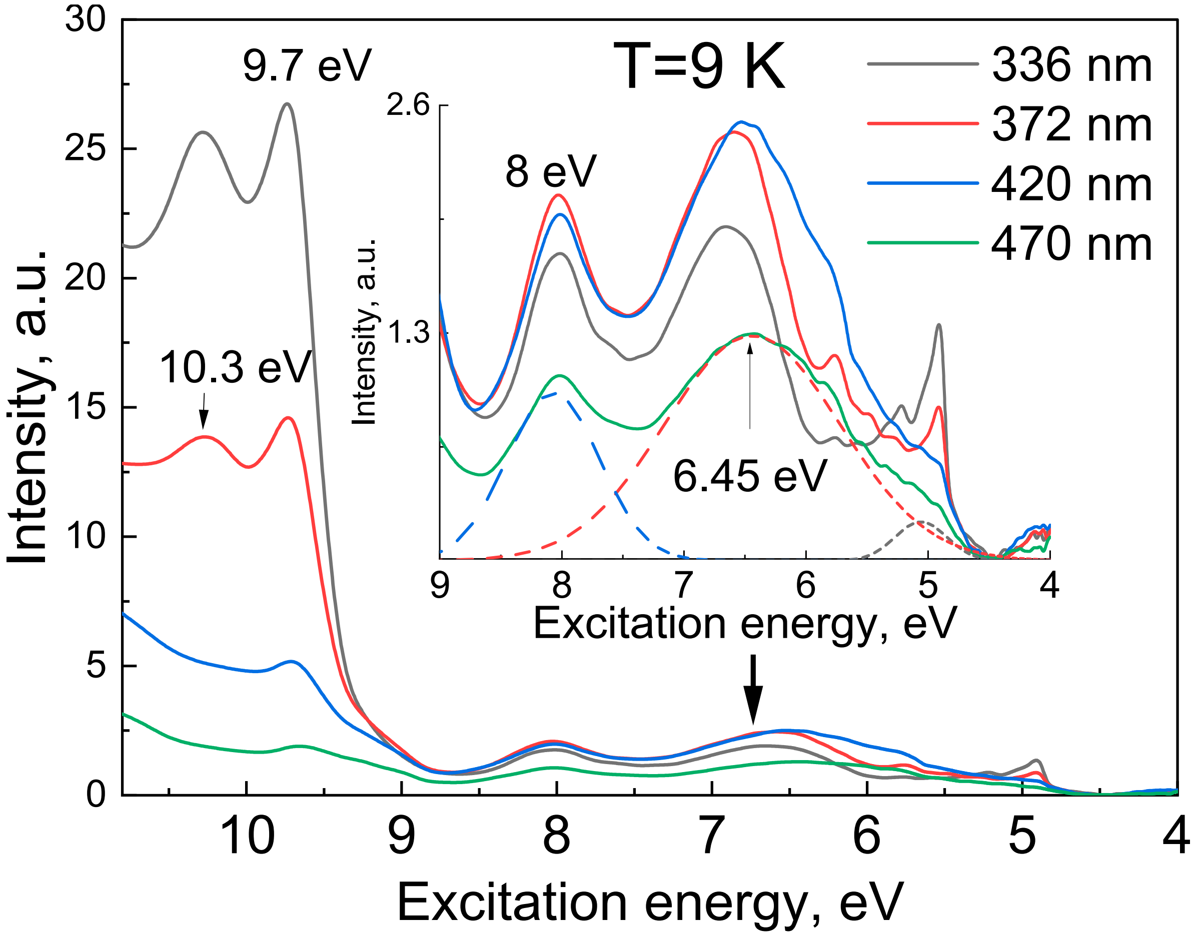

Figure 4. Excitation spectra of $BaMgF_4$ ceramics at T = 9 K for various emission wavelengths: 336 nm, 372 nm, 420 nm, and 470 nm. The inset highlights the energy range from 9 to 4 eV (dashed blue and red lines Gaussian decomposition components).

These observed features highlight the complex excitation dynamics in $BaMgF_4$ ceramics, in which the interplay of excitonic transitions, intermediate states, and possible defect-related levels leads to distinct luminescent responses at different emission wavelengths and excitation energies.

A detailed examination of the luminescence of $BaMgF_4$ ceramics under excitation at different photon energies at T = 9 K revealed a multicomponent emission spectrum structure dependent on the excitation energy (Figure 5). The luminescence spectra, analyzed using Gaussian decomposition, showed emission maxima at 3.71, 3.55, 3.33, 3, and ~2.8 eV.

Under excitation at 6.6 eV (Figure 5a), the emission spectrum consisted of several overlapping bands, with the primary maximum located at 3.33 eV. Additional emission bands were observed at both higher and lower energies, indicating the involvement of multiple relaxation mechanisms for the excited states. This suggests the presence of excitonic transitions and contributions from other states within the crystal lattice.

When the excitation energy increased to 9.7 eV (Figure 5b), the luminescence intensity significantly increased, reflecting the more efficient excitation of transitions near the band edge and additional excited states. The dominant emission peak shifted to 3.71 eV, while spectral components observed under lower excitation energy remained present. Notably, the low-energy components around 3 eV and 2.81 eV became more pronounced.

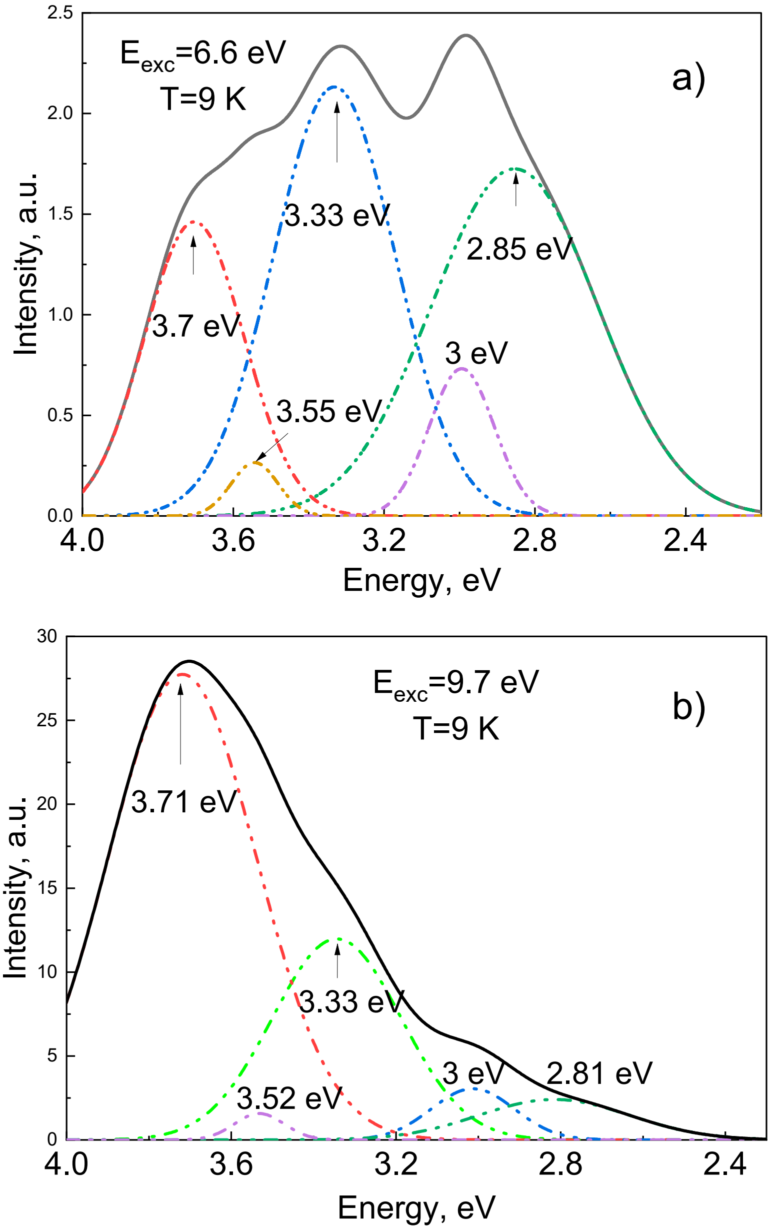

Figure 5. Luminescence spectra of $BaMgF_4$ under excitation at 6.6 eV (**a**) and 9.7 eV (**b**) (black line -measured spectra, dashed multicolor lines—Gaussian components).

4. Discussion

In $BaMgF_4$ ceramics, excitation mechanisms proceed as follows: when photon energy $h\nu \geq Eg$ (approximately 9.5–10.3 eV), an electron is directly excited from the valence band to the conduction band. Following this excitation, in ionic crystals with a wide bandgap, excitons often form. Free excitons migrate through the crystal, facilitating energy transfer, a process known as energy migration. Additionally, in the ionic matrix, excitons may undergo self-trapping, localizing at fluorine clusters or lattice defects, forming self-trapped excitons (STE).

Based on the analysis of the luminescence and excitation spectra across various energy regions, the luminescence mechanism of $BaMgF_4$ ceramics can be described as follows. The bandgap of $BaMgF_4$ was estimated to be approximately 10.3 eV, as determined using the numerically discrete variational (DV-Xα) method, according to [39]. The luminescence bands with maxima at 330, 370, 420, and 470 nm (3.71, 3.55, 3.33, 3, and ~2.8 eV) are associated with different mechanisms of excitation and relaxation of excited states.

The primary luminescence band at 330 nm corresponds to excitonic transitions. Exciton excitation predominantly occurs near the edge of the fundamental absorption at 9.3 eV, with a maximum light yield observed at 9.7 eV (Figure 4). This indicates the excitation of interband transitions and the formation of self-trapped excitons (STE), which subsequently relax and emit in the ultraviolet region. The luminescence band near 370 nm is attributed to defects in the crystal lattice, as evidenced by its efficient excitation at 6.7 eV and 8 eV, as well as by high-energy photons at 10.3 eV. Excitation at energies of 6.45 eV and 8 eV, according to [40–42], is presumably associated with oxygen-related defect centers. The synthesis of $BaMgF_4$ in an ambient air atmosphere inevitably leads to oxygen incorporation into the structure, forming defects related to oxygen. These oxygen-related defects play a crucial role in the luminescence behavior of the material. Emission linked to such defects is observed at wavelengths of 370 nm and 420 nm, where the primary excitation channels include direct excitation and energy transfer through exciton migration. Figure 6 presents an energy diagram of $BaMgF_4$ ceramics, illustrating the proposed mechanisms of electronic excitation relaxation.

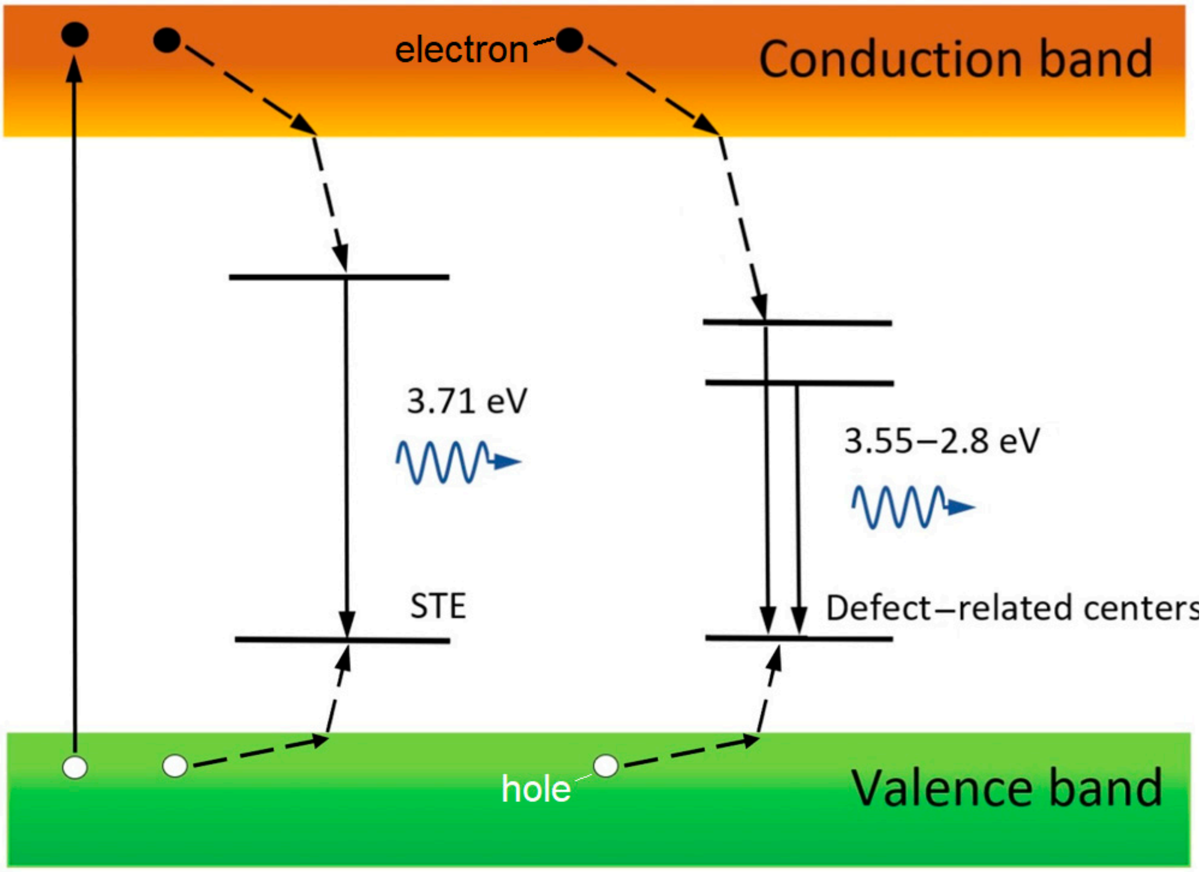

Figure 6. Energy scheme of excitation and relaxation processes in $BaMgF_4$ ceramics.

The increase in emission intensity at 370 nm and 420 nm compared to 330 nm under these excitation energies suggests a dominant contribution of defect centers in this spectral range (Figure 5). The primary channel for defect excitation involves energy transfer from excitons via their migration through the lattice. This assumption is supported by the varying PL intensities at different excitation energies, where the highest luminescence output is observed near 10.3 eV, corresponding to exciton formation.

In the excitation spectra of 330 nm and 370 nm, extrema at 9.7 eV and 10.3 eV are observed. At 9.7 eV, the exciton energy is lower than the energy required for direct electron transition to the conduction band, as part of the energy is expended to form a bound excitonic state [14]. The transition at 10.3 eV may correspond to high-energy excitonic states or electron-phonon interactions. Alternatively, it could result from interband transitions between various subzones in the conduction and valence bands.

The possible mechanisms for low-energy photon excitation include defect state excitation and charge-transfer transitions. In $BaMgF_4$, charge transfer between anions (F^-) and cations (Ba^{2+} or Mg^{2+}) can occur at lower energies, contributing to the observed luminescence.

Thus, the dynamics of excitation and luminescence in $BaMgF_4$ ceramics are determined by the combined contributions of interband transitions, self-trapped excitons, and defect states, which are characteristic of wide-band fluoride materials.

Future research will focus on the detailed determination of the positions of the luminescence bands identified in this work using a comprehensive approach, including thermally stimulated luminescence (TSL), electron paramagnetic resonance (EPR), and first-principles quantum chemical calculations.

5. Conclusions

The novelty of this study lies in the first-time investigation of undoped $BaMgF_4$ ceramics under synchrotron excitation in the vacuum ultraviolet (VUV) region. This approach highlighted unique luminescent properties driven by intrinsic defects and excitonic processes, which were previously unexplored for $BaMgF_4$ in its undoped form. Using synchrotron radiation provided a tunable, high-intensity excitation source, enabling detailed analysis of electronic transitions and defect-related states. Additionally, this study used electron beam synthesis with intrinsic defect centers that significantly affect luminescence, further distinguishing this study from previous work focusing on doped or alternative fluoride systems.

This investigation of $BaMgF_4$ ceramics revealed a complex interplay between interband transitions, excitonic processes, and defect-related luminescence, defining the material's unique optical properties. The primary luminescence band at 330 nm is attributed to the formation of self-trapped excitons (STE), excited efficiently near the band edge at 9.3–9.7 eV, indicating strong interband transitions and subsequent excitonic relaxation. The dominance of this band highlights the significant role of excitonic processes in the ultraviolet region.

In addition to excitonic luminescence, bands at 370, 420, and 470 nm are associated with defect states, such as F-centers and their configurations (e.g., F_2 centers). These defect-related emissions are effectively excited at 6.45 eV, 8 eV, and through high-energy photons at 10.3 eV, underscoring the impact of structural and oxygen-related defects introduced during synthesis. The excitation spectrum further reveals distinct maxima at 5, 6.45, and 8 eV, linked to defect-related absorption processes. These findings suggest that energy transfer mechanisms, such as exciton migration, play a crucial role in exciting defect states, contributing to the observed luminescent dynamics.

The use of radiation synthesis through high-energy electron beam irradiation has proven effective in introducing defect centers into the material. These defects not only enhance luminescence properties but also broaden the potential applications of $BaMgF_4$ ceramics in UV and VUV optical devices. The controlled introduction of defects offers a pathway to tuning luminescent properties for specific technological needs, such as scintillators, lasers, and advanced photonic systems.

Overall, the combined contributions of interband transitions, excitonic relaxation, and defect-related luminescence establish $BaMgF_4$ ceramics as a versatile material with significant potential for applications in ultraviolet and vacuum ultraviolet spectral regions.

Author Contributions: Conceptualization, A.M.Z.; data curation, A.V.S., R.N.K., and Y.S.; formal analysis, Z.T.K., A.A., R.N.K., and A.I.P.; investigation, K.K.K., and M.T.K.; methodology, A.M.Z., Z.T.K., A.A., M.T.K., and A.I.P.; project administration, A.M.Z.; resources, A.A., and M.T.K.; software, K.K.K.; validation, R.N.K., and Y.S.; visualization, A.V.S., Z.T.K., K.K.K., and Y.S.; writing—original draft, A.M.Z., and A.V.S.; writing—review and editing, A.M.Z., Z.T.K., and A.I.P. All authors have read and agreed to the published version of the manuscript.

Funding: This research was funded by the Committee of Science of the Ministry of Science and Higher Education of the Republic of Kazakhstan (Grant No. AP14871114). In addition, Anatoli Popov was supported by Latvian research project lzp-2023/1-0453 "Prediction of long-term stability of functional materials under extreme radiation conditions" and the Latvian State Research Program No. VPP-IZM-CERN-2022/1-0001.

Data Availability Statement: The raw data supporting the conclusions of this article will be made available by the authors on request.

Acknowledgments: We acknowledge DESY (Hamburg, Germany), a member of the Helmholtz Association HGF, for the provision of experimental facilities. This research was carried out at the P66 beamline at PETRA III. Beamtime was allocated for proposals I-20231405.

Conflicts of Interest: The authors declare no conflicts of interest.

References

1. Wu, A.; Wang, Z.; Su, L.; Jiang, D.; Zou, Y.; Xu, J.; Chen, J.; Ma, Y.; Chen, X.; Hu, Z. Crystal Growth and Frequency Conversion of BaMgF$_4$ Single Crystal by Temperature Gradient Technique. *Opt. Mater. Amst.* **2014**, *38*, 238–241. [CrossRef]
2. Buchter, S.C.; Fan, T.Y.; Liberman, V.; Zayhowski, J.J.; Rothschild, M.; Mason, E.J.; Cassanho, A.; Jenssen, H.P.; Burnett, J.H. Periodically Poled BaMgF$_4$ for Ultraviolet Frequency Generation. *Opt. Lett.* **2001**, *26*, 1693. [CrossRef]
3. Kim, S.W.; Chang, H.Y.; Halasyamani, P.S. Selective Pure-Phase Synthesis of the Multiferroic BaMF$_4$ (M = Mg, Mn, Co, Ni, and Zn) Family. *J. Am. Chem. Soc.* **2010**, *132*, 17684–17685. [CrossRef]
4. Hayashi, T.; Yoshihara, M.; Ohmi, S.; Tokumitsu, E.; Ishiwara, H. Electrical Properties of Ferroelectric BaMgF$_4$ Films Grown on GaAs Substrates Using AlGaAs Buffer Layer. *Appl. Surf. Sci.* **1997**, *117–118*, 418–422. [CrossRef]
5. Muñoz-Santiuste, J.E.; Loro, H.; Marino, R.; Goldner, P.; Vasyliev, V.; Víllora, E.G.; Shimamura, K.; Molina, P.; Ramírez, M.O.; Bausá, L.E. Local environment of optically active Nd^{3+} ions in the ultratransparent BaMgF$_4$ ferroelectric crystal. *Phys. Rev. B* **2012**, *85*, 184110. [CrossRef]
6. Dejneka, M.; Snitzer, E.; Riman, R.E. Blue, Green and Red Fluorescence and Energy Transfer of Eu^{3+} in Fluoride Glasses. *J. Lumin.* **1995**, *65*, 227–245. [CrossRef]
7. Fujihara, S.; Kishiki, Y.; Kimura, T. Sol–Gel Processing of BaMgF$_4$–Eu^{2+} Thin Films and Their Violet Luminescence. *J. Alloys Compd.* **2002**, *333*, 76–80. [CrossRef]
8. Kore, B.P.; Kumar, A.; Erasmus, L.; Kroon, R.E.; Terblans, J.J.; Dhoble, S.J.; Swart, H.C. Energy Transfer Mechanisms and Optical Thermometry of BaMgF$_4$:Yb^{3+},Er^{3+} Phosphor. *Inorg. Chem.* **2018**, *57*, 288–299. [CrossRef]
9. Shimamura, K.; Vıllora, E.G.; Muramatsu, K.; Ichinose, N. Advantageous growth characteristics and properties of SrAlF$_5$ compared with BaMgF$_4$ for UV/VUV nonlinear optical applications. *J. Cryst. Growth* **2005**, *275*, 128–134. [CrossRef]
10. Jansons, J.; Rachko, Z.; Valbis, J.; Andriessen, J.; Dorenbos, P.; van Eijk, C.W.E.; Khaidukov, N.M. Cross-Luminescence of Complex Halide Crystals. *J. Phys. Condens. Matter* **1993**, *5*, 1589–1596. [CrossRef]
11. Yamaga, M.; Hattori, K.; Kodama, N.; Ishizawa, N.; Honda, M.; Shimamura, K.; Fukuda, T. Superlattice Structure of Ce^{3+} -Doped BaMgF$_4$ Fluoride Crystals—X-Ray Diffraction, Electron Spin-Resonance, and Optical Investigations. *J. Phys. Condens. Matter* **2001**, *13*, 10811–10824. [CrossRef]
12. Yanagida, T.; Kawaguchi, N.; Fujimoto, Y.; Sugiyama, M.; Furuya, Y.; Kamada, K.; Yokota, Y.; Yoshikawa, A.; Chani, V. Growth and Scintillation Properties of BaMgF$_4$. *Nucl. Instrum. Methods Phys. Res. A* **2010**, *621*, 473–477. [CrossRef]
13. Trevisani, M.; Ivanovskikh, K.; Ramírez, M.; Molina, P.; Víllora, E.; Shimamura, K.; Bausá, L.; Bettinelli, M. Bettinelli. VUV–UV 5d–4f interconfigurational transitions of Nd^{3+} in BaMgF$_4$ ferroelectric crystals. *J. Lumin.* **2014**, *153*, 136–139. [CrossRef]
14. Pustovarov, V.A.; Ogorodnikov, I.N.; Omelkov, S.I.; Isaenko, L.I.; Yelisseyev, A.P.; Goloshumova, A.A.; Lobanov, S.I.; Krinitsyn, P.G. Electronic Excitations and Luminescence of SrMgF$_4$ Single Crystals. *Phys. Solid State* **2014**, *56*, 456–467. [CrossRef]
15. Hayashi, E.; Ito, K.; Yabashi, S.; Yamaga, M.; Kodama, N.; Ono, S.; Sarukura, N. Ultraviolet Irradiation Effect of Ce^{3+}-Doped BaMgF$_4$ Crystals. *J. Alloys Compd.* **2006**, *408–412*, 883–885. [CrossRef]

16. Kodama, N.; Hoshino, T.; Yamaga, M.; Ishizawa, N.; Shimamura, K.; Fukuda, T. Optical and Structural Studies on BaMgF4:Ce^{3+} Crystals. *J. Cryst. Growth* **2001**, *229*, 492–496. [CrossRef]
17. Preishuber-Pflügl, F.; Wilkening, M. Evidence of low dimensional ion transport in mechanosynthesized nanocrystalline $BaMgF_4$. *Dalton Trans.* **2014**, *43*, 9901–9908. [CrossRef]
18. Sayed, F.N.; Mandal, B.P.; Jayakumar, O.D.; Arya, A.; Kadam, R.M.; Dixit, A.; Naik, R.; Tyagi, A.K. Rare examples of fluoride-based multiferroic materials in Mn-substituted $BaMgF_4$ systems: Experimental and theoretical studies. *Inorg. Chem.* **2011**, *50*, 11765–11772. [CrossRef]
19. Gingl, F. $BaMgF_4$ and $Ba_2Mg_3F_{10}$: New examples for structural relationships between hydrides and fluorides. *Z. Für Anorg. Und Allg. Chem.* **1997**, *623*, 705–709. [CrossRef]
20. Janssens, S.; Williams, G.V.M.; Clarke, D. Synthesis and characterization of rare earth and transition metal doped $BaMgF_4$ nanoparticles. *J. Lumin.* **2013**, *134*, 277–283. [CrossRef]
21. Kannan, C.V.; Shimamura, K.; Zeng, H.R.; Kimura, H.; Villora, E.G.; Kitamura, K. Ferroelectric and anisotropic electrical properties of $BaMgF_4$ single crystal for vacuum UV devices. *J. Appl. Phys.* **2008**, *104*, 114115. [CrossRef]
22. Bergman, J.G.; Crane, G.R.; Guggenheim, H. Linear and nonlinear optical properties of ferroelectric $BaMgF_4$ and $BaZnF_4$. *J. Appl. Phys.* **1975**, *46*, 4645–4646. [CrossRef]
23. Jian, G.; Liu, M.; Chen, W.; Yan, C.; Wong, C.P. Orientational dependences of optical properties in $BaMgF_4$. *Opt. Mater.* **2018**, *86*, 471–474. [CrossRef]
24. Sinharoy, S.; Buhay, H.; Francombe, M.H.; Takei, W.J.; Doyle, N.J.; Rieger, J.H.; Stepke, E. Growth and characterization of ferroelectric $BaMgF_4$ films. *J. Vac. Sci. Technol. A Vac. Surf. Film.* **1991**, *9*, 409–413. [CrossRef]
25. Rey, J.M.; Bill, H.; Lovy, D.; Hagemann, H. Europium doped $BaMgF_4$, an EPR and optical investigation. *J. Alloys Compd.* **1998**, *268*, 60–65. [CrossRef]
26. Quilty, J.W.; Edgar, A.; Schierning, G. Photostimulated luminescence and thermoluminescence in europium-doped barium magnesium fluoride. *Curr. Appl. Phys.* **2008**, *8*, 420–424. [CrossRef]
27. Singh, V.S.; Belsare, P.D.; Moharil, S.V. Wet chemical synthesis and study of luminescence in some Eu^{2+} activated $AEMgF_4$ hosts. *Phys. Solid. State* **2020**, *62*, 2318–2324. [CrossRef]
28. Usseinov, A.B.; Karipbayev, Z.T.; Purans, J.; Kakimov, A.B.; Bakytkyzy, A.; Zhunusbekov, A.M.; Koketai, T.A.; Kozlovskyi, A.L.; Suchikova, Y.; Popov, A.I. Study of β-Ga2O3 Ceramics Synthesized under Powerful Electron Beam. *Materials* **2023**, *16*, 6997. [CrossRef]
29. Koketai, T.A.; Strelkova, A.V.; Zhunusbekov, A.M.; Karipbayev, Z.T.; Lisitsyna, L.A.; Chakin, A.M. Luminescent Properties of $BaxMg_{(2-x)}F_4$:W Ceramics. *Eurasian J. Phys. Funct. Mater.* **2023**, *7*, 2. [CrossRef]
30. Strelkova, A.V.; Lisitsyn, V.M.; Lisitsyna, L.A.; Koketai, T.A.; Mussakhanov, D.A.; Karipbayev, Z.T.; Zhunusbekov, A.M. Characterization and Luminescence Dynamics of MgF_2:W Ceramics. *Eurasian J. Phys. Funct. Mater.* **2023**, *7*, 4. [CrossRef]
31. Omelkov, S.I.; Chernenko, K.; Ekström, J.C.; Jurgilaitis, A.; Khadiev, A.; Kivimäki, A.; Kotlov, A.; Kroon, D.; Larsson, J.; Nagirnyi, V.; et al. Recent Advances in Time-Resolved Luminescence Spectroscopy at MAX IV and PETRA III Storage Rings. *J. Phys. Conf. Ser.* **2022**, *2380*, 012135. [CrossRef]
32. Kappelhoff, J.; Keil, J.N.; Kirm, M.; Makhov, V.N.; Chernenko, K.; Möller, S.; Jüstel, T. Spectroscopic studies on Pr^{3+} doped YPO_4 and $LuPO_4$ upon vacuum ultraviolet (VUV) and synchrotron radiation excitation. *Chem. Phys.* **2022**, *562*, 111646. [CrossRef]
33. Pankratova, V.; Chernenko, K.; Bocharov, D.; Chesnokov, A.; Sychikova, Y.; Popov, A.I.; Pankratov, V. Unveiling of UV intrinsic luminescence in $(Lu,Y)_2SiO_5$:Ce^{3+} single crystals. *Opt. Mater.* **2024**, *152*, 115554. [CrossRef]
34. Zhunusbekov, A.M.; Karipbayev, Z.T.; Tolegenova, A.; Kumarbekov, K.K.; Nurmoldin, E.E.; Baizhumanov, M.M.; Kotlov, A.; Popov, A.I. Comparative VUV synchrotron excitation study of YAG:Eu and YAG:Cr ceramics. *Crystals* **2024**, *14*, 897. [CrossRef]
35. Kuzmin, A.; Pankratov, V.; Kalinko, A.; Kotlov, A.; Shirmane, L. UV-VUV synchrotron radiation spectroscopy of $NiWO_4$. *Fiz. Nizk. Temp.* **2016**, *42*, 694–698. [CrossRef]
36. Lisitsyn, V.M.; Musakhanov, D.A.; Korzhneva, T.G.; Strelkova, A.V.; Lisitsyna, L.A.; Golkovsky, M.G.; Zhunusbekov, A.M.; Karipbaev, J.T.; Kozlovsky, A.L. Synthesis and Characterization of Ceramics BaxMg(2−x)F_4 Activated by Tungsten. *Glass Phys. Chem.* **2023**, *49*, 288–292. [CrossRef]
37. Lisitsyn, V.; Tulegenova, A.; Golkovski, M.; Polisadova, E.; Lisitsyna, L.; Mussakhanov, D.; Alpyssova, G. Radiation Synthesis of High-Temperature Wide-Bandgap Ceramics. *Micromachines* **2023**, *14*, 2193. [CrossRef]
38. Ermolayev, A.V.; Tulegenova, A.T.; Lisitsyna, L.A.; Korzhneva, T.G.; Lisitsyn, V.M. The Influence of the Initial Charge Compaction on the Radiation Synthesis of YAG:Ce Ceramics. *Russ. Phys. J.* **2022**, *64*, 1692–1696. [CrossRef]
39. Kang, L.L.; Liu, T.Y.; Zhang, Q.R.; Xu, L.Z.; Zhang, F.W. Study on the Electronic Structures and Absorption Bands of $BaMgF_4$ Crystal with F Color Centre. *Chin. Phys. B* **2011**, *20*, 047101. [CrossRef]
40. Egranov, A.V.; Radzhabov, E.A. *Spectroscopy of Oxygen and Hydrogen Impurity Centers in Alkali Halide Crystals*; Nauka: Moscow, Russia, 1992; p. 161.

41. Radzhabov, E.; Otroshok, V. Optical Spectra of Oxygen Defects in BaFCl and BaFBr Crystals. *J. Phys. Chem. Solids* **1995**, *56*, 1–7. [CrossRef]
42. Radzhabov, E. Oxygen Defects in Fluoride Crystals. *Mater. Sci. Forum* **1997**, *239–241*, 261–266. [CrossRef]